Appl. Phys. B 64, 647–650 (1997)

Applied Physics B Lasers and Optics

Excited state absorption measurements and laser potential of Cr^{4+} doped Ca_2GeO_4

T.C. Brunold[1], H.U. Güdel[1], M.F. Hazenkamp[1], G. Huber[2], S. Kück[2]

[1] Departement für Chemie und Biochemie, Universität Bern, Freiestrasse 3, CH-3000 Bern 9, Switzerland
(Fax: +41-31/631-3993, E-mail: guedel@iac.unibe.ch)
[2] Institut für Laser-Physik, Universität Hamburg, Jungiusstraße 9a, D-20355 Hamburg, Germany
(Fax: +49-40/4123-6281, E-mail: kueck@physnet.uni-hamburg.de)

Received: 28 October 1996

Abstract. Polarized continuous wave excited state absorption (ESA) measurements on Cr^{4+} doped Ca_2GeO_4 in the 450–2000 nm spectral region at room temperature are presented. Weak ESA bands due to the $^3T_2 \rightarrow {}^3T_1(F)$ transition are observed between 1200 and 2000 nm and stronger ESA bands due to $^3T_2 \rightarrow {}^3T_1(P)$ peak below 1200 nm. The overlap of the $^3T_2 \rightarrow {}^3T_1(F)$ ESA band with the emission which extends from 1100 to about 1600 nm will significantly affect the laser performance of Cr^{4+} doped Ca_2GeO_4. The effective peak stimulated emission cross section at 1350 nm in $\mathbf{E}\|\mathbf{b}$ polarization is only about 3×10^{-20} cm^2. However, our results indicate that tunable laser action between 1300 and 1500 nm should, in principle, be possible.

PACS: 42.70; 78.45; 78.50

Since the demonstration of near infrared (NIR) laser action of Cr doped Mg_2SiO_4 [1] and the definite assignment of the lasing ion to Cr^{4+} in tetrahedral oxo coordination [2] the spectroscopic and laser properties of many Cr^{4+} doped materials have been investigated [3]. The most important Cr^{4+} doped laser materials up till now are Mg_2SiO_4 (forsterite) and $Y_3Al_50_{12}$(YAG). However, these materials suffer from serious drawbacks. One of the problems is the efficient nonradiative relaxation leading to low quantum efficiencies at room temperature of 9% and 14-22%, respectively [3, 4]. A second problem is the difficulty to achieve high concentrations of Cr^{4+} in these hosts without simultaneously incorporating large amounts of Cr^{3+}.

The optical spectroscopic properties of Cr^{4+} doped Ca_2GeO_4 have been studied in great detail [5, 6]. Ca_2GeO_4 has the olivine structure and is thus isomorphic with forsterite [7]. The absorption and luminescence spectra were found to be very similar to those of Cr^{4+} doped forsterite, the only difference being a red shift of all spin allowed transitions of some 1300 cm^{-1} due to the smaller ligand field strength. An important advantage of Cr^{4+} doped Ca_2GeO_4 is the much weaker temperature quenching of the Cr^{4+} luminescence compared with Cr^{4+} doped forsterite; at room temperature the quantum efficiency is estimated to be about 60%. Moreover, high Cr^{4+} concentrations are easily achieved in the Ca_2GeO_4 lattice and no indication for the presence of Cr^{3+} was found in the absorption and luminescence spectra [5, 6].

Recently, laser action of a Cr^{4+} doped Ca_2GeO_4 crystal was demonstrated [8]. Pulsed laser action was observed upon pumping at 1064 nm with a Q-switched Nd:YAG laser. The free-running laser output was centred at 1400 nm. In the present paper we explore the excited state absorption properties of Cr^{4+} doped Ca_2GeO_4 which, for the $LiAlO_2$, and $LiGaO_2$ hosts, have been shown to represent a limiting factor for laser operation [9]. ESA at the pump or lasing wavelength strongly affects the lasing threshold and the slope efficiency. Thus, these spectra provide valuable information on the possible tuning range and on the suitable wavelengths for efficient pumping.

1 Experimental

Ca_2GeO_4 has the olivine structure and crystallizes in the orthorhombic space group Pnmb [7]. The Cr^{4+} ion substitutes for Ge^{4+} which occupies a tetrahedrally oxo coordinated site of C_s symmetry. Single crystals Ca_2GeO_4 doped with 0.5 mole% Cr^{4+} were grown from a $CaCl_2$ flux by slowly cooling from 1250 to 800 °C at -2.5 °C/h. Best results were obtained using the weight composition CaO (15%), GeO_2 (14%), and $CaCl_2 \cdot 2H_2O$ (71%). Chromium was added in the form of Cr_2O_3 and CrO_3 in the molar $Cr^{3+} : Cr^{6+}$ ratio 2 : 1. The Cr concentration in the flux was 0.5 mole% with respect to Ge. By comparison of the absorption coefficient of the crystal with that published in the literature [6] it appears that practically all the Cr is build into the crystal as Cr^{4+}. The optical axes of the crystals with dimensions up to $7 \times 5 \times 4$ mm^3 were determined with a polarization microscope. They were assigned to crystallographic axes by comparing the polarized absorption spectra with published spectra [6].

Ground state absorption spectra were measured on a Cary 5e double beam spectrophotometer. Spontaneous emission spectra were measured upon excitation with xenon lamp in combination with a KG 3 filter glass and a water bath. The emitted light was dispersed by a 0.75 m single monochro-

mator and detected by a Ge detector. The ESA spectra were obtained with the pump and probe technique by measuring the transmission spectrum and the difference in transmission of the pumped and the unpumped crystal as described in detail in Ref. [10]. Pumping was performed with a Nd:YAG laser operating at 1064 nm with an output power 1 W. The transmitted probe beam of a tungsten lamp (250 W) was dispersed by a 0.5 m single monochromator and detected with either a Si diode or a cooled InSb detector. It can be shown that [10]:

$$\frac{I_\mathrm{p}-I_\mathrm{u}}{I_\mathrm{u}} \approx c(\sigma_\mathrm{GSA}+\sigma_\mathrm{SE}-\sigma_\mathrm{ESA}) \qquad (1)$$

where $I_{\mathrm{p(u)}}$ is the transmitted intensity in the pumped (unpumped) case, c is a constant and σ_GSA, σ_SE and σ_ESA are the cross sections for ground state absorption, stimulated emission and excited state absorption, respectively. Positive $(I_\mathrm{p}-I_\mathrm{u})/I_\mathrm{u}$ values correspond to the situation that ground state bleaching or stimulated emission are stronger than excited state absorption, whereas negative values occur if excited state absorption dominates.

2 Results

Figure 1 shows the ground state absorption spectra at room temperature of Cr^{4+} doped Ca_2GeO_4 for **E**$\|$**b** and **E**$\|$**c** polarizations in the VIS and NIR. The spectra are similar to those which were published before [5, 6]. Two rather intense bands at 810 and 740 nm in **E**$\|$**b** and **E**$\|$**c** polarization, respectively, are adjacent to much weaker bands between 850 and 1250 nm. The **E**$\|$**a** polarization which is not presented here shows a single absorption band centered at 630 nm. In this polarization we observe only very weak NIR absorption which would prevent efficient pumping with a Nd:YAG laser or available laser diodes at 808 and 960 nm. Moreover, **E**$\|$**a** polarized emission is almost absent and we thus restrict ourselves to the **E**$\|$**b** and **E**$\|$**c** polarizations.

The spontaneous emission spectra for **E**$\|$**b** and **E**$\|$**c** polarizations at room temperature are shown in Fig. 2. The luminescence is predominantly **E**$\|$**b** polarized. The polarization ratio between the **E**$\|$**b** and **E**$\|$**c** polarizations is about 2 : 1. The luminescence decay times at 10 K and at room temperature are 25 µs and 15 µs, respectively [5, 6].

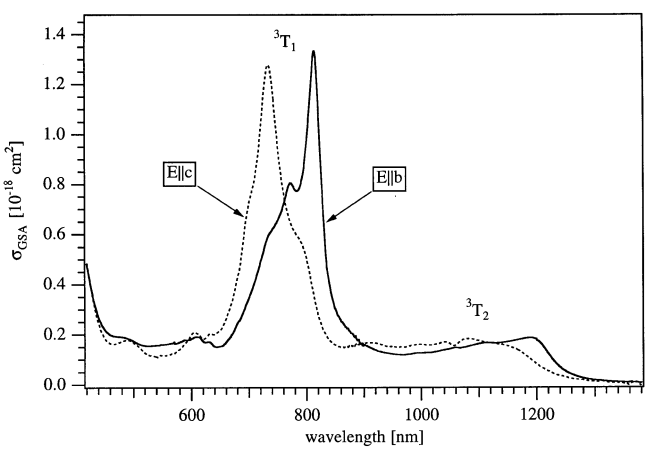

Fig. 1. Ground state absorption spectra at room temperature for **E**$\|$**b** and **E**$\|$**c** polarizations of Cr^{4+} doped Ca_2GeO_4

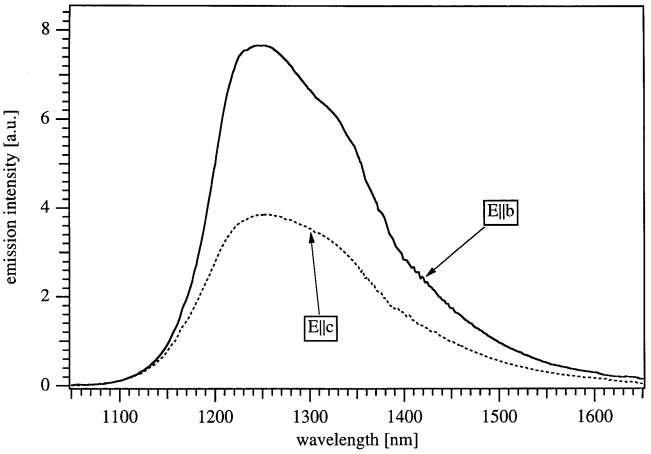

Fig. 2. Spontaneous emission spectra at room temperature for **E**$\|$**b** and **E**$\|$**c** polarizations of Cr^{4+} doped Ca_2GeO_4

ESA spectra at room temperature were measured for **E**$\|$**b** and **E**$\|$**c** polarizations. The polarized $(I_\mathrm{p}-I_\mathrm{u})/I_\mathrm{u}$ spectra are shown in Fig. 3. For both polarizations the signal is positive between 450 and 1500 nm, indicating that ESA is not dominating in this spectral range. GSA bleaching bands are found between 450 and 1200 nm which correspond to the bands in the GSA absorption spectra in Fig. 1. Below 450 nm the onset of a strong ESA band is observed. Above 1400 nm weak broad ESA bands appear in both polarizations. For **E**$\|$**b** we find a weak positive signal between 1200 and 1500 nm. Since this signal more or less coincides with the spontaneous emission spectrum and since there is no GSA a longer wavelengths than 1300 nm we assign this band to stimulated emission. It is likely attenuated by the superimposed ESA, which becomes dominant above 1500 nm.

3 Discussion

In Ca_2GeO_4 the Cr^{4+} ion ($3d^2$) is in a tetrahedral oxo coordination with a $^3A_2$ ground state, a $^3T_2$ emitting state, and the higher excited spin triplet states $^3T_1(F)$ and $^3T_1(P)$. However, the tetrahedron is distorted and the true site symmetry is C_s. This leads to orbital splittings of the T states in T_d symmetry. A detailed assignment of the GSA spectrum of Cr^{4+} doped Ca_2GeO_4 was given in Ref. [6]. The strong bands in Fig. 1 at 630, 810, and 740 nm in **E**$\|$**a** (not shown), **E**$\|$**b** and **E**$\|$**c** polarization, respectively, are due to the transitions from the $^3A_2$ ground state to three orbital components of the $^3T_1(F)$ excited state. The bands between 900 and 1200 nm are due to transitions to the three orbital components of the $^3T_2$ state. The predominantly **c** polarized weak band at 490 nm is assigned to a component of the $^3T_1(P)$ state.

The luminescence transition is from the lowest crystal field component of the $^3T_2$ state to the $^3A_2$ ground state. The decay time of 25 µs at 10 K is essentially radiative [5]. The band shape of the spontaneous luminescence on the short wavelength side is slightly affected by reabsorption of the emitted light by the material itself. Because of the small Stokes shift and the thermal broadening of the absorption and emission bands at room temperature there is a rather large spectral overlap between absorption and luminescence [5] which leads to reabsorption and thus a lower luminescence intensity on the

Table 1. Predicted spectral positions and polarization behaviour of ESA transitions in Cr^{4+} doped Ca_2GeO_4 based on ground state absorption data [6]. The metastable state is at 8340 cm^{-1} above the ground state

ESA transition $^3A''(^3T_2)_{\text{metastable}}\longrightarrow$	energy [cm^{-1}]/ wavelength [nm]	polarization
$^3_aA''[(^3T_1)(F)]$	3980/2510	**E**$\|$**b,a**
$^3A'[(^3T_1)(F)]$	5210/1920	**E**$\|$**c**
$^3_bA''[(^3T_1)(F)]$	7450/1340	**E**$\|$**b,a**
$^3_aA''[(^3T_1)(P)]$	10620/940	**E**$\|$**b,a**
$^3A'[(^3T_1)(P)]$	12160/820	**E**$\|$**c**
$^3_bA''[(^3T_1)(P)]$	12329/810	**E**$\|$**b,a**
LMCT state	34700/290	**E**$\|$**a,b,c**

short wavelength side. This effect is smaller for lower Cr^{4+} concentrations and smaller crystals. Reabsorption is expected to have a detrimental effect on the laser performance on the short wavelength side of the emission, as was shown before for Cr^{4+} doped forsterite [11].

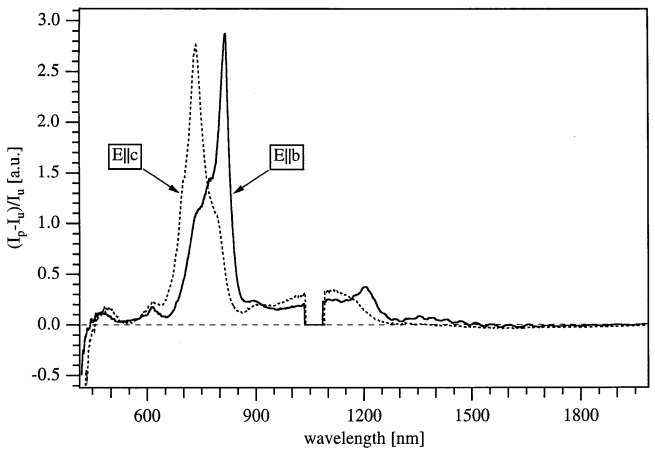

Fig. 3. $(I_p-I_u)/I_u$ spectra at room temperature for **E**$\|$**b** and **E**$\|$**c** polarizations of Cr^{4+} doped Ca_2GeO_4. Between 1030 nm and 1080 nm the pump beam at 1064 nm was blocked in order to protect the detector

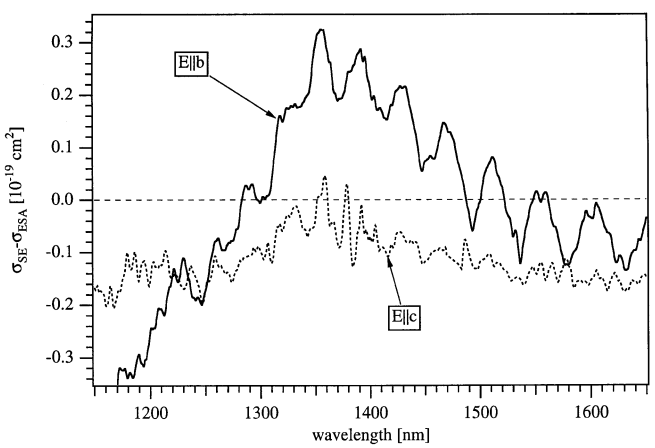

Fig. 4. σ_{SE}-σ_{ESA} spectra at room temperature in the spectral region of the stimulated emission for **E**$\|$**b** and **E**$\|$**c** polarizations of Cr^{4+} doped Ca_2GeO_4 obtained after subtraction of the σ_{GSA} spectra from the appropriately scaled spectra in Fig. 3

From the GSA spectra and from the selection rules in C_s symmetry [6] we can predict the band positions and polarizations of the ESA transitions. This has been done for the spin and electric dipole allowed transitions from the metastable $^3A''(^3T_2)$ state at 8340 cm^{-1} above the $^3A_2$ ground state (and thus 270 cm^{-1} below the next higher component of $^3T_2$) to the various components of $^3T_1(F)$, $^3T_1(P)$, and ligand-to-metal charge transfer (LMCT) states, see Table 1. On the basis of this table we assign the weak broad ESA bands above 1400 nm to transitions to the components of $^3T_1(F)$ and the onset of the strong ESA band below 450 nm to a transition to the first LMCT state. Apparently, the GSA cross sections between 700 and 1000 nm are much larger than those of the $^3T_2 \rightarrow {}^3T_1(P)$ ESA transitions so that the latter cannot be observed in Fig. 3. The stimulated emission band between 1250 and 1500 nm in **E**$\|$**b** polarization more or less coincides with the spontaneous emission (see Fig. 2).

In order to reveal any ESA bands which are hidden under the GSA bleaching bands in Fig. 3 we subtracted the GSA spectrum from the $(I_p-I_u)/I_u$ spectrum. Calibration of the $(I_p-I_u)/I_u$ spectrum was performed with the help of the GSA bleaching signal between 600 and 900 nm. After subtraction of the GSA spectrum from the appropriately scaled $(I_p-I_u)/I_u$ spectrum we obtain the $\sigma_{EFF}=\sigma_{SE}-\sigma_{ESA}$ spectrum. The σ_{EFF} spectrum in the region of the stimulated emission is shown in Fig. 4. In the spectral region between 500 nm and 1100 nm we find broad ESA bands with σ_{ESA} on the order of 1×10^{-19} cm^2. On the basis of Table 1 these bands are readily assigned to $^3T_2 \rightarrow {}^3T_1(P)$. Note that the cross sections of the GSA bands in this region are an order of magnitude larger (Fig. 1), so that efficient pumping between 500 and 1100 nm should be possible.

In the σ_{EFF} spectrum for **E**$\|$**b** the SE has its maximum at about 1350 nm. σ_{EFF} at 1350 nm is roughly 3×10^{-20} cm^2 (see Fig. 4). However, this SE band is clearly overlapped by a broad ESA band since the σ_{EFF} signal is negative below 1300 nm and above 1500 nm. In **E**$\|$**c** polarisation the emission is even weaker than for **E**$\|$**b** (see Fig. 2) so that for **E**$\|$**c** $\sigma_{SE}<\sigma_{ESA}$ and σ_{EFF} is negative over the whole spectral range of the emission. This is in agreement with the data in Table 1, where we predict the ESA transition to the $_b{}^3A''$ component of $^3T_1(F)$ at 1340 nm in **E**$\|$**b,a** polarizations. In **E**$\|$**c** polarisation the weak SE band is overlapped by the tails of the broad ESA bands to the $^3A'[(^3T_1)(F)]$ and $^3A'[(^3T_1)(P)]$ states at 1920 nm and 820 nm, respectively. We can compare the measured σ_{EFF} at 1350 nm with the σ_{SE} calculated from the radiative luminescence decay time using [12]:

$$\frac{1}{\tau_{rad}}=\frac{8\pi n^2}{\lambda^2}\sigma_{SE}(1350\text{nm})\Delta\nu \qquad (2)$$

where τ_{rad} is the radiative lifetime (25×10^{-6} s), λ is the wavelength at the maximum (1350×10^{-9} m), n is the refractive index (1.73 [5]) and $\Delta\nu$ is the effective luminescence band width (4.1×10^{13} Hz). Hence, σ_{SE}(1350 nm) is about 2×10^{-19} cm^2, roughly a factor 7 larger than the measured value of σ_{EFF} of 3×10^{-20} cm^2 in **E**$\|$**b** polarisation. Thus, at 1350 nm, the maximum of the stimulated emission band, the output is reduced by a factor of 7 as a result of ESA.

We expect that this will detrimentally affect the laser performance of Cr^{4+} doped Ca_2GeO_4. However, tunable laser action should, in principle, be possible because $\sigma_{SE}>\sigma_{ESA}$

between 1300 and 1500 nm. This is in agreement with the reported wavelength of the free running laser at 1400 nm [8]. Note that the situation is different from that of Cr^{4+} doped forsterite where σ_{SE} at the maximum of the SE band was measured to be 1.8×10^{-19} cm^2 in Ref. [11] and 4×10^{-19} cm^2 in Ref. [13]. Both values are in good agreement with the value calculated from the radiative lifetime of 2×10^{-19} cm^2, so that ESA plays no significant role in that case. The onset of ESA was reported at longer wavelengths than 1300 nm [11, 13]. For Cr^{4+} doped $LiAlO_2$ and $LiGaO_2$, however, ESA overlapping with the luminescence was also observed. In that case it was found that $\sigma_{ESA} > \sigma_{SE}$ over the whole spectral range of the emission, thus inhibiting room temperature laser action [9].

4 Conclusions

Though the room temperature luminescence of Cr^{4+} doped Ca_2GeO_4 is much less quenched in comparison with Cr^{4+} doped forsterite the ESA bands overlapping the emission significantly reduce the laser potential of this material. The effective peak stimulated emission cross section at 1350 nm is only 3×10^{-20} cm^2 and thus almost one order of magnitude lower than for Cr^{4+} doped forsterite. However, since high Cr^{4+} concentrations are easily achieved without significant luminescence quenching and diode pumping at 800 nm and 1 µm is possible, Cr^{4+} doped Ca_2GeO_4 may have some potential as microchip or waveguide laser material.

Acknowledgements. Financial support from the Human Capital and Mobility program of the European Union and the Swiss National Science Foundation are gratefully acknowledged.

References

1. V. Petricevic, S.K. Gayen, R.R. Alfano: Appl. Phys. Lett. **53**, 2590 (1988);
H.R. Verdun, L.M. Thomas, D.M. Andraukas, T. McCollum, A. Pinto: Appl. Phys. Lett. **53**, 2593 (l988)
2. T.S. Rose, R.A. Fields, M.H. Whitmore, D.J. Singel: J. Opt. Soc. Am. B **11**, 428 (l994)
3. R. Moncorgée, H. Manaa, G. Boulon: Opt. Mater. **4**, 139 (l994)
4. H. Eilers, U. Hömmerich, S.M. Jacobsen, W.M. Yen, K.R. Hoffman, W. Jia: Phys. Rev. B **49**, 15505 (1994);
S. Kück, K. Petermann, U. Pohlmann, G. Huber: Phys. Rev. B **51**, 17323 (l995)
5. M.F. Hazenkamp, U. Oetliker, U. Kesper, D. Reinen, H.U. Güdel: Chem. Phys. Lett. **233**, 466 (l995)
6. M.F. Hazenkamp, H.U. Güdel, M. Atanasov, U. Kesper, D. Reinen: Phys. Rev. B **53**, 2367 (l996)
7. U. Shikegazu, U. Kazuyori, K.K. Keiichi: Semento Gijutsu Nenpo **29**, 32 (l975)
8. V. Petricevic, A.B. Bykov, R.R. Alfano: *Postdeadline paper PD2-2 of the Advanced Solid-State Lasers Conference*, San Francisco (1996)
9. S. Hartung, S. Kück, T. Danger, K. Petermann, G. Huber: in *Advanced Solid-State Lasers, Vol.1 of Trends in Optics and Photonics*, S.A. Payne, C.R. Pollock, eds. (Optical Society of America, Washington D.C., 1996) p.90
10. J. Koetke, G. Huber: Appl. Phys. B **61**, 151 (1995)
11. V. Petricevic, A. Seas, R.R. Alfano: in *Advanced Solid-State Lasers, Vol.6 of the OSA Proceedings Series*, H.P. Jenssen, G. Dubé, eds. (Optical Society of America, Washington D.C., 1990) p.73
12. L.D. Merkle, A. Guyot, B.H.T. Chai: J. Appl. Phys. **77**, 474 (1995)
13. N.K. Kuleshov, V.G. Shcherbitsky, V.P. Mikhailov, S. Hartung, T. Danger, S. Kück, K. Petermann, G. Huber: in *Advanced Solid-State Lasers. Vol.1 of Trends in Optics and Photonics*, S.A. Payne, C.R. Pollock, eds. (Optical Society of America, Washington D.C., 1996) p.85
14. V. Petricevic, A.B. Bykov, J.M. Evans, R.R. Alfano: Opt. Lett. **21**, 1750 (1996)

Note added in proof

After acceptance of this manuscript for publication, we became aware of a very recent report an room-temperature near-infrared tunable laser application of Cr^{4+} doped Ca_2GeO_4 [14]. Tunability over the 1348–1482 nm spectral range with a maximum slope efficiency of 6.1% was demonstrated. These results are in excellent agreement with our predictions.